Supporting Information: Sharma et al.
Activity-Based Protein Profiling shows heterogeneous signaling adaptations to BRAF inhibition.

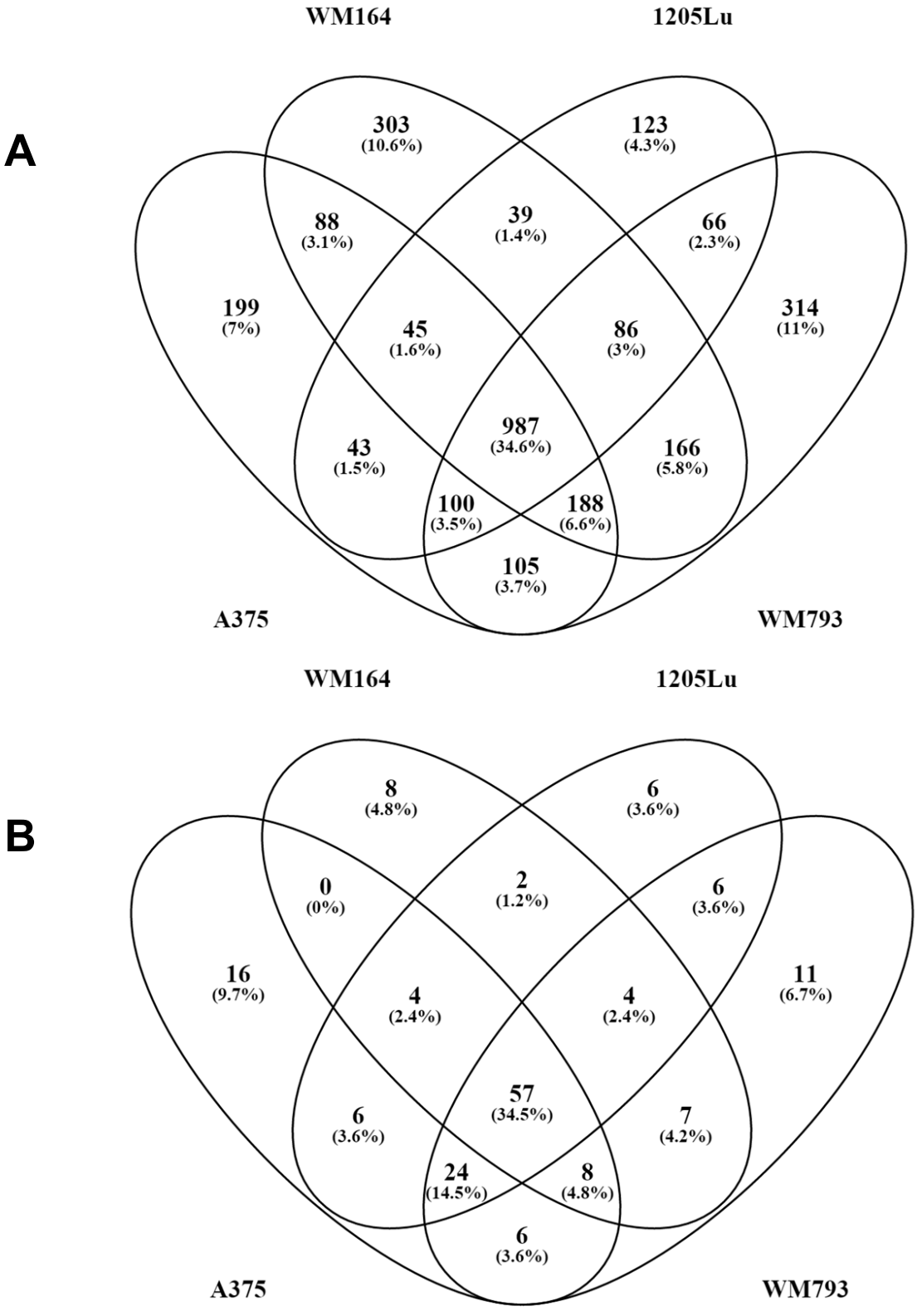

Supplementary Figure S1. Venn Diagrams showing unique and common proteins **(A)** and kinases **(B)** identified from each cell line model.

Supporting Information: Sharma et al.
Activity-Based Protein Profiling shows heterogeneous signaling adaptations to BRAF inhibition.

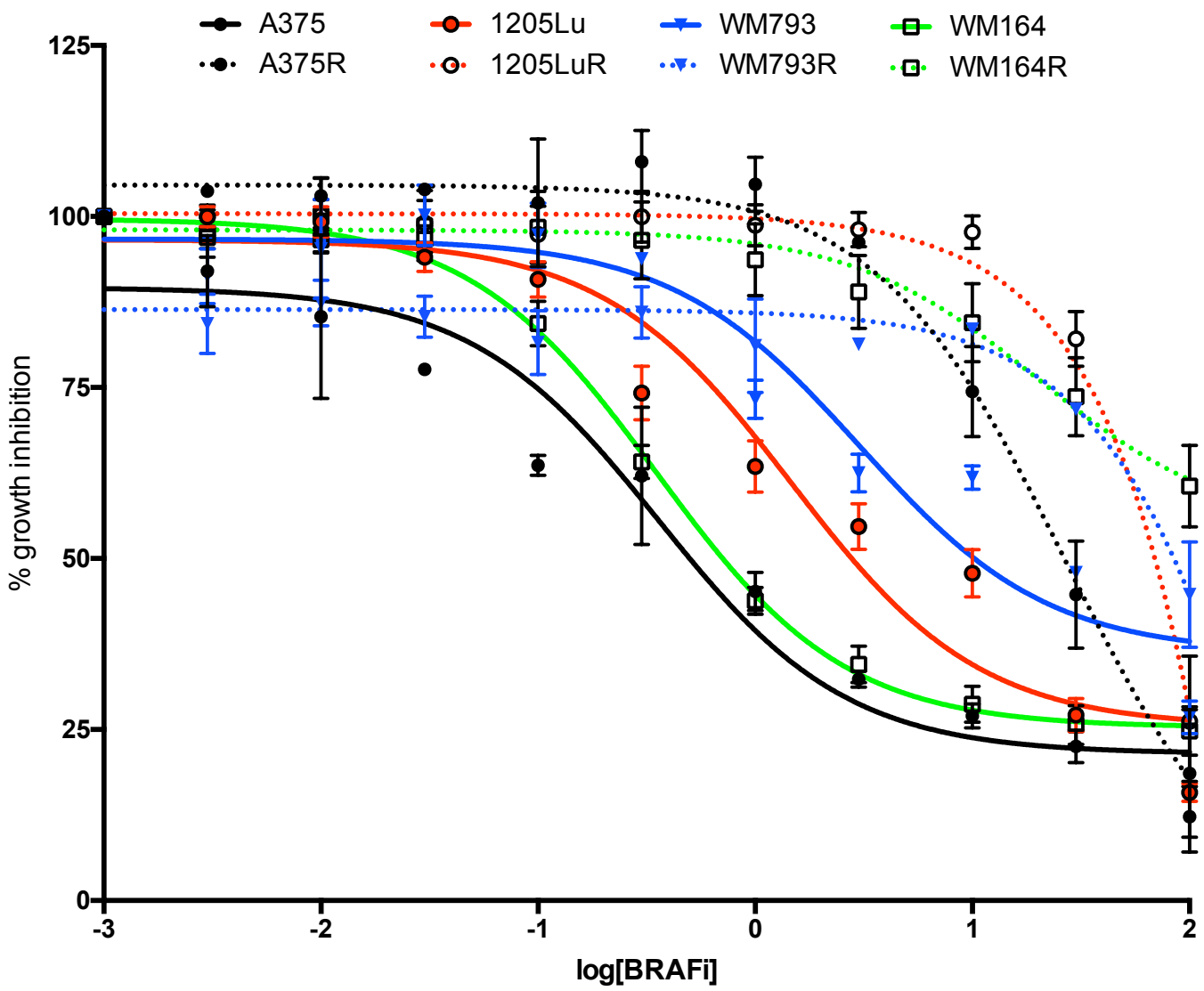

	A375	A375R	WM793	WM793R	1205Lu	1205LuR	WM164	WM164R
LogIC50	-0.444	1.433	0.4816	2.628	0.1673	~ 4.993	-0.4535	1.31
IC50 (uM vemurafenib)	0.3598	27.11	3.031	424.6	1.47	~ 98481	0.352	20.4
Std. Error (LogIC50)	0.1468	0.1129	0.1572	1.186	0.07972	~ 112.6	0.05007	0.2726
Goodness to Fit (R square)	0.9191	0.9553	0.9055	0.7867	0.8936	0.7884	0.9454	0.3801

Supplementary Figure S2. MTT Assay showing BRAF inhibitor dose response curves in naïve and BRAFi resistant cells. Cells were treated with increasing doses of vemurafenib for 72 hours then incubated with MTT reagent for 2-3 hours. Media was removed and crystals were re-solubilized using DMSO., then absorbance was read at 490 nm. Data is normalized to respective cell line controls.

Supporting Information: Sharma et al.
Activity-Based Protein Profiling shows heterogeneous signaling adaptations to BRAF inhibition.

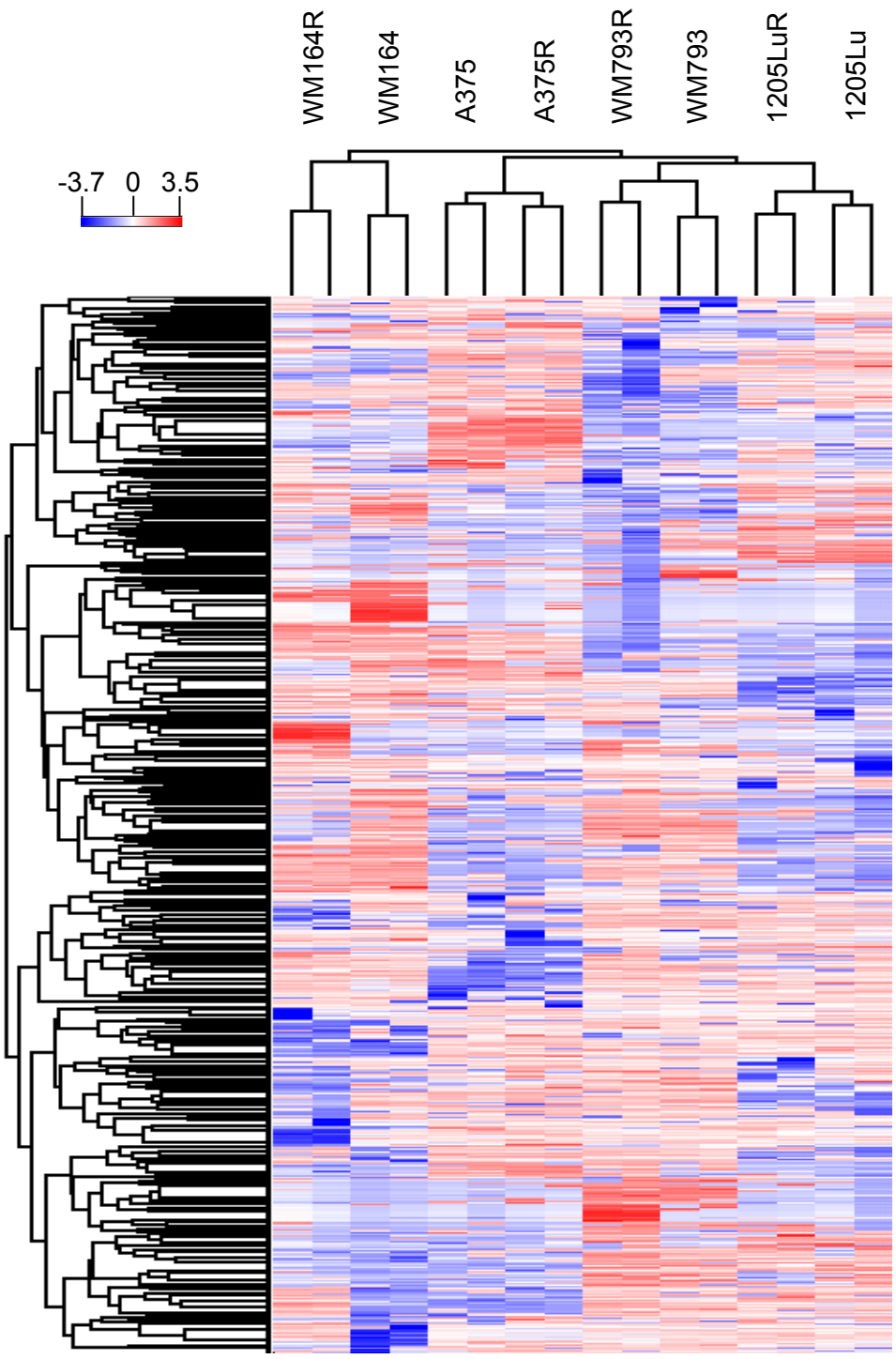

Supplementary Figure S3. Heat map of all the desthiobiotinylated (DBT) peptides observed between naïve and BRAFi resistant cells produced by unsupervised clustering.

Supporting Information: Sharma et al.
Activity-Based Protein Profiling shows heterogeneous signaling adaptations to BRAF inhibition.

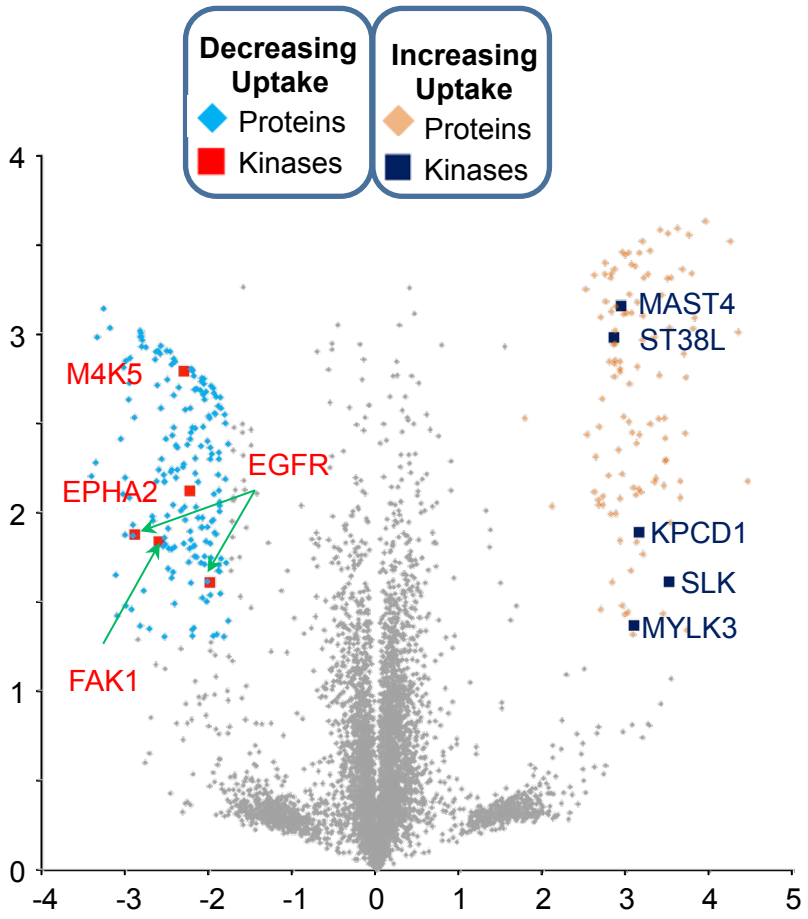

Supplementary Figure S4: Comparison of Peptides Representing ATP Probe Uptake by Kinases in Naïve and BRAFi Resistant A375 Melanoma Cell Line. Volcano plot of DBT-peptides observed in A375 naïve and BRAFi resistant cells using the following cutoffs: log2 ratio exceeds 2 standard deviations away from the mean and p value < 0.05.

Supporting Information: Sharma et al.
Activity-Based Protein Profiling shows heterogeneous signaling adaptations to BRAF inhibition.

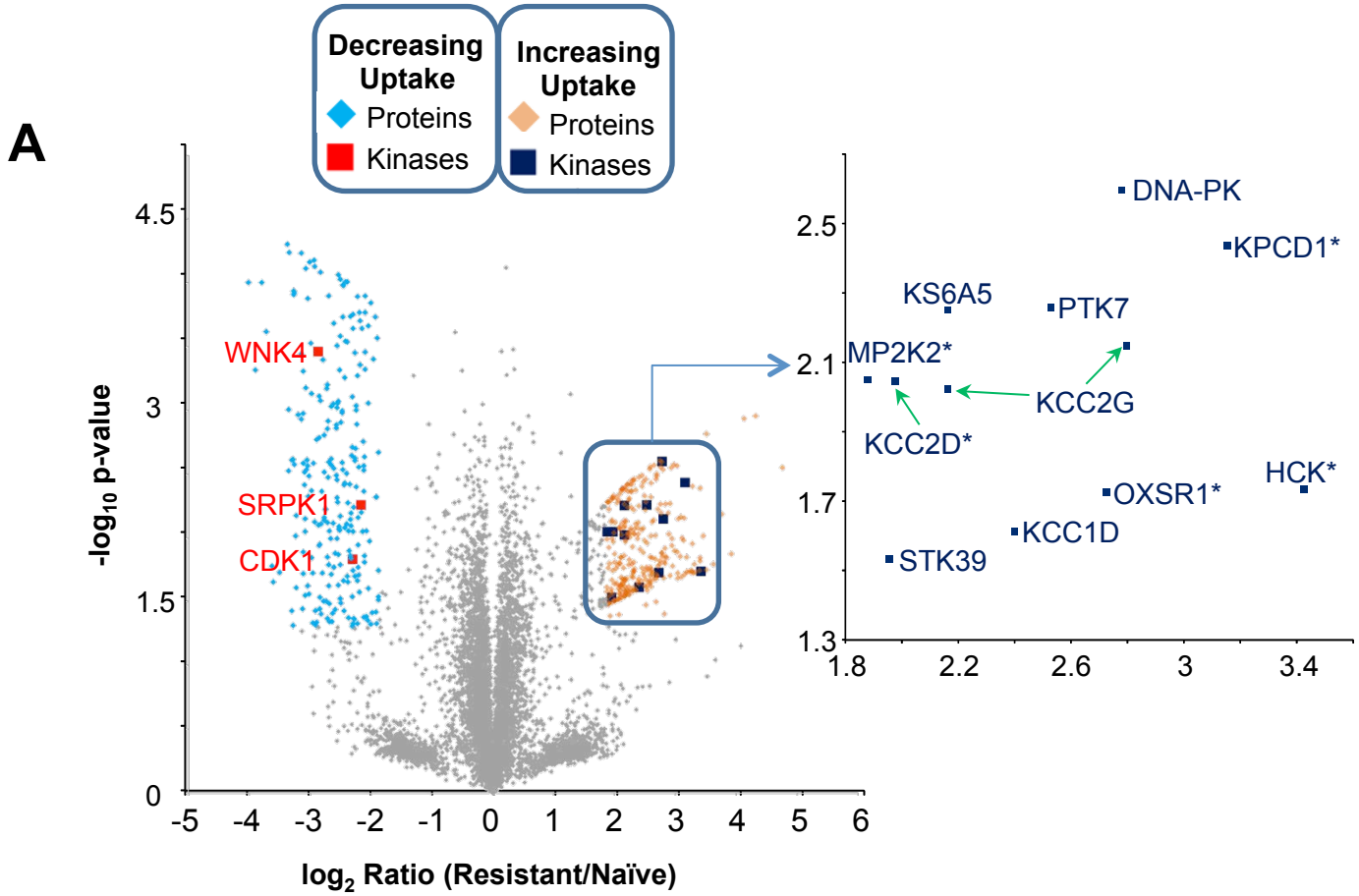

Supplementary Figure S5: Comparison of Peptides Representing ATP Probe Uptake by Kinases in Naïve and BRAFi Resistant WM793 Melanoma Cell Line. Volcano plot of DBT-peptides observed in WM793 naïve and BRAFi resistant cells **(A)** using the following cutoffs: log2 ratio exceeds 2 standard deviations away from the mean and p-value < 0.05, inset shows kinases with significantly increased ATP probe uptake in the WM793 BRAFi resistant cell line, * represent a non-unique kinase (Supplementary Table 6). **(B)** Interactome of uniquely mapped kinases with increased ATP uptake in the WM793 BRAFi resistant cell line (p-value < 0.05),. Proteins with unconnected nodes (PTK7, CaMK II gamma, ULK3, NEK9, ROCK2, MAST3, MEK6, CaMK1D) not shown for clarity.

Supporting Information: Sharma et al.
Activity-Based Protein Profiling shows heterogeneous signaling adaptations to BRAF inhibition.

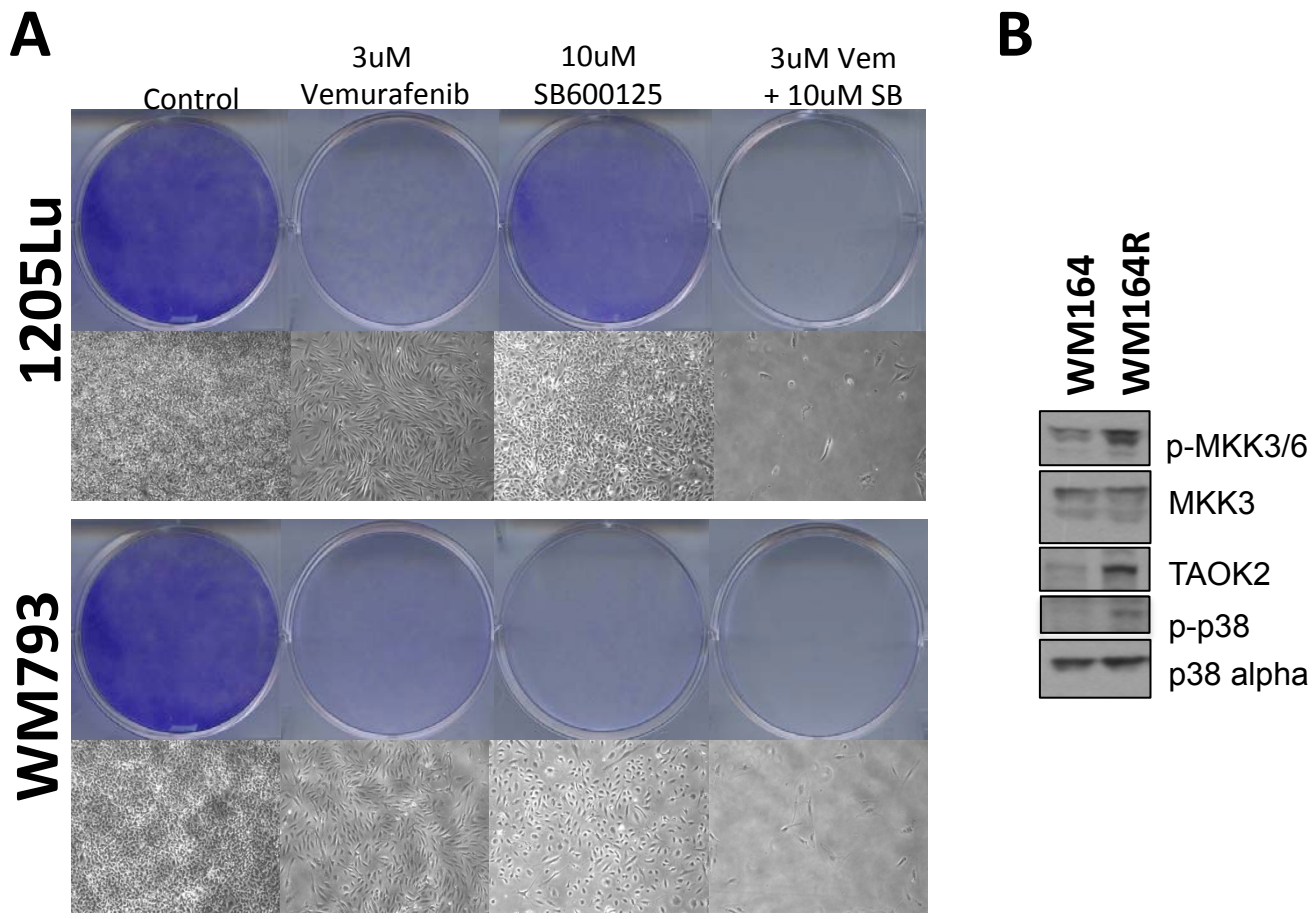

Supplementary Figure S6: Combining BRAF and JNK Inhibition. (A) Long term colony formation assays show increased BRAF inhibitor sensitivity with combined JNK inhibition. Crystal violet stain of WM793 and 1205Lu cells treated with 3μM vemurafenib and 10μM SB431542 for 2 weeks. **(B)** Western blot analysis showing levels of phospho-MKK3/6, MKK3, TAOK2, phospho-p38, and p38 alpha between WM164 and WM164R.

Supporting Information: Sharma et al.
Activity-Based Protein Profiling shows heterogeneous signaling adaptations to BRAF inhibition.

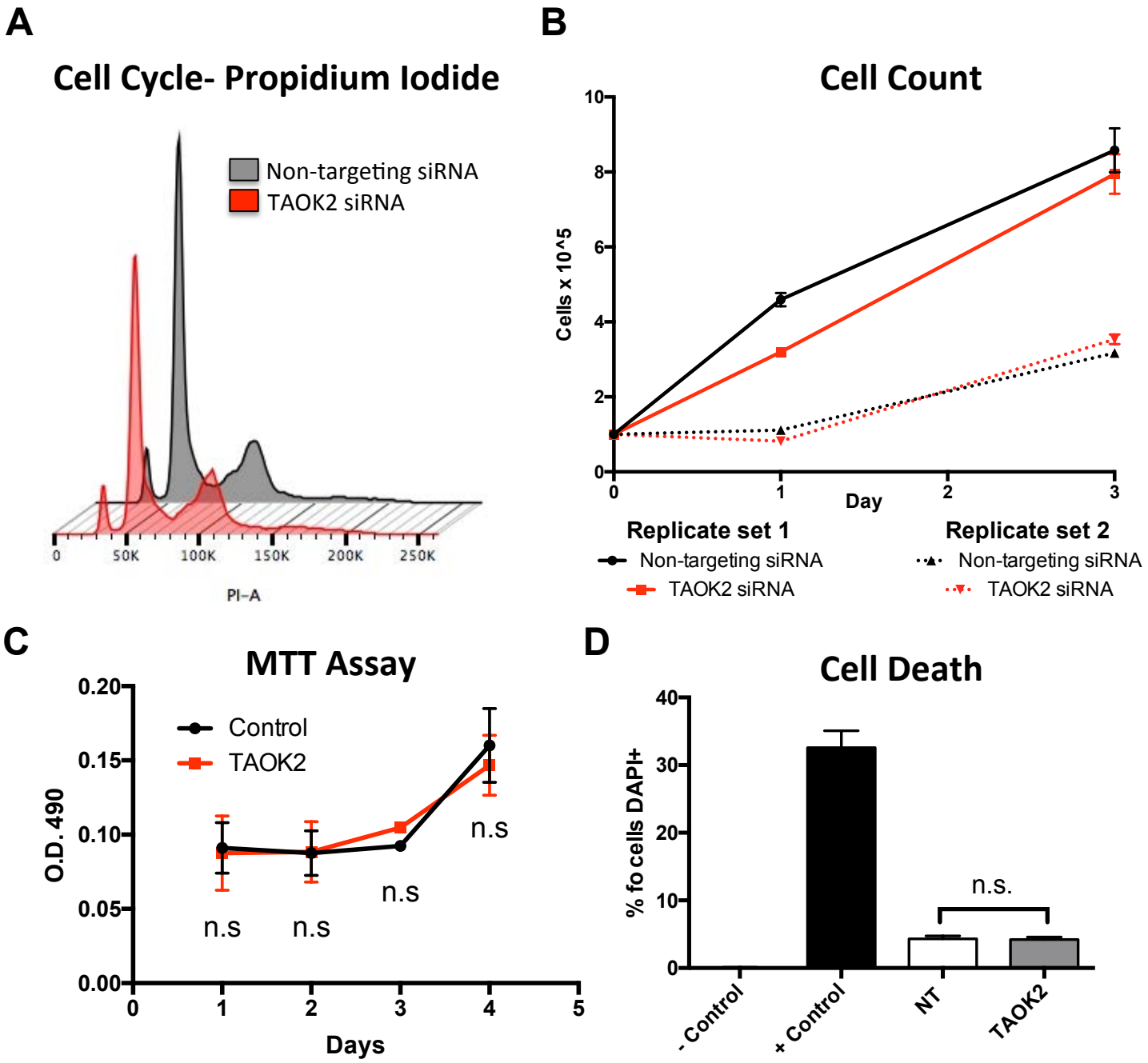

Supplementary Figure S7: Role of TAOK2 in growth and proliferation of WM164R. (A) WM164R cells transfected with non-targeting and TAOK2-targeting siRNAs. Cells were fixed, stained with PI (485 uL PBS, 10uL PI 1mg/ml, 5uL RNAse 25mg/ml per sample) and then analyzed using flow cytometry. Representative histograms for PI-Area shown. **(B)** Cells were counted following transfection. **(C)** MTT growth assay was carried out following transfection. **(D)** Cells were treated with 3μM BRAFi vemurafenib following transfection, stained with DAPI, and then analyzed by flow cytometry. For comparison, positive (+) and negative (-) staining controls were included (WM164R cells heated to 95C for 2 minutes then incubated with or without DAPI). All experiments were carried out in duplicate.

Supporting Information: Sharma et al.
Activity-Based Protein Profiling shows heterogeneous signaling adaptations to BRAF inhibition.

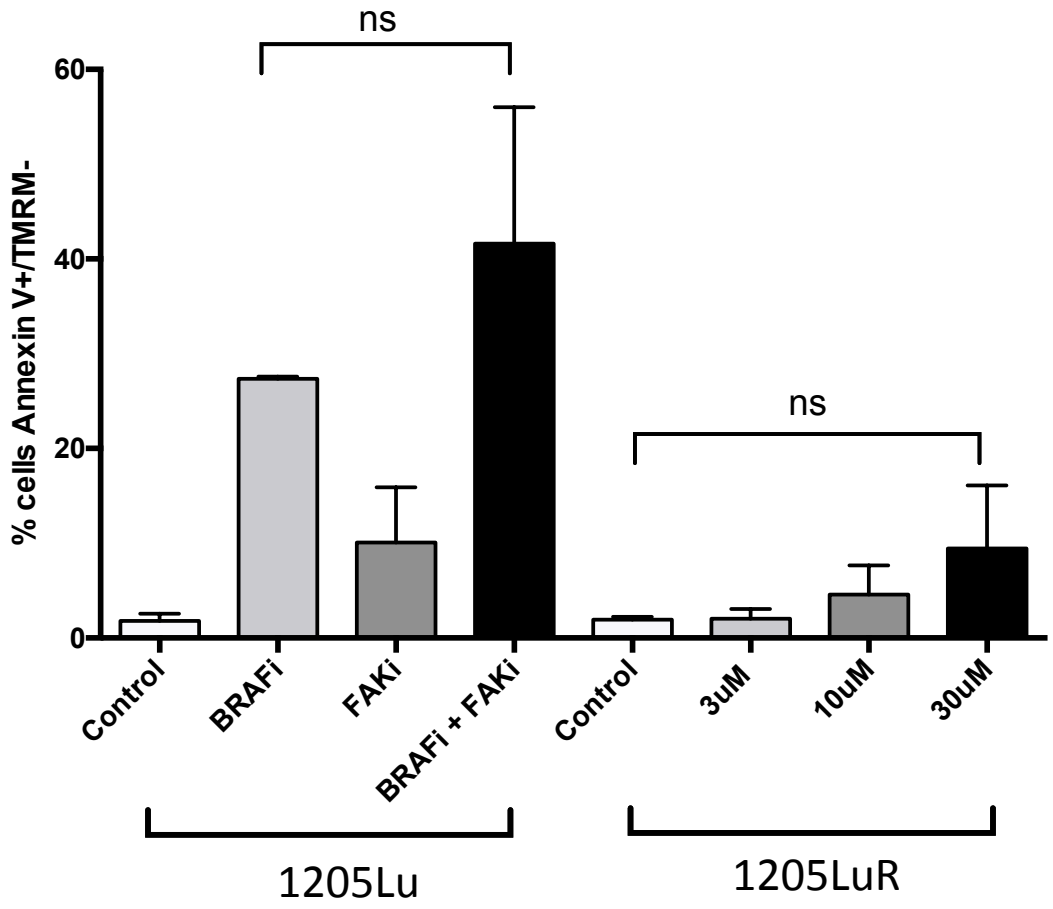

Supplementary Figure S8: Effects of FAK inhibition on BRAFi sensitivity. 1205Lu cells were treated with 3μM BRAFi vemurafenib, 10μM FAKi PF573228, or the combination of BRAF+FAKi. 1205LuR cells were treated with increasing concentrations of FAKi PF573228. Cells were treated for 72 hours then stained for Annexin V and TMRM and analyzed by flow cytometry. Bar graph shows percentage of cells that are Annevin V+ and TMRM- (apoptotic cells). Significance measured by unpaired t-test in GraphPad Prism (GraphPad Software Inc, La Jolla, CA).

Supporting Information: Sharma et al.
Activity-Based Protein Profiling shows heterogeneous signaling adaptations to BRAF inhibition.

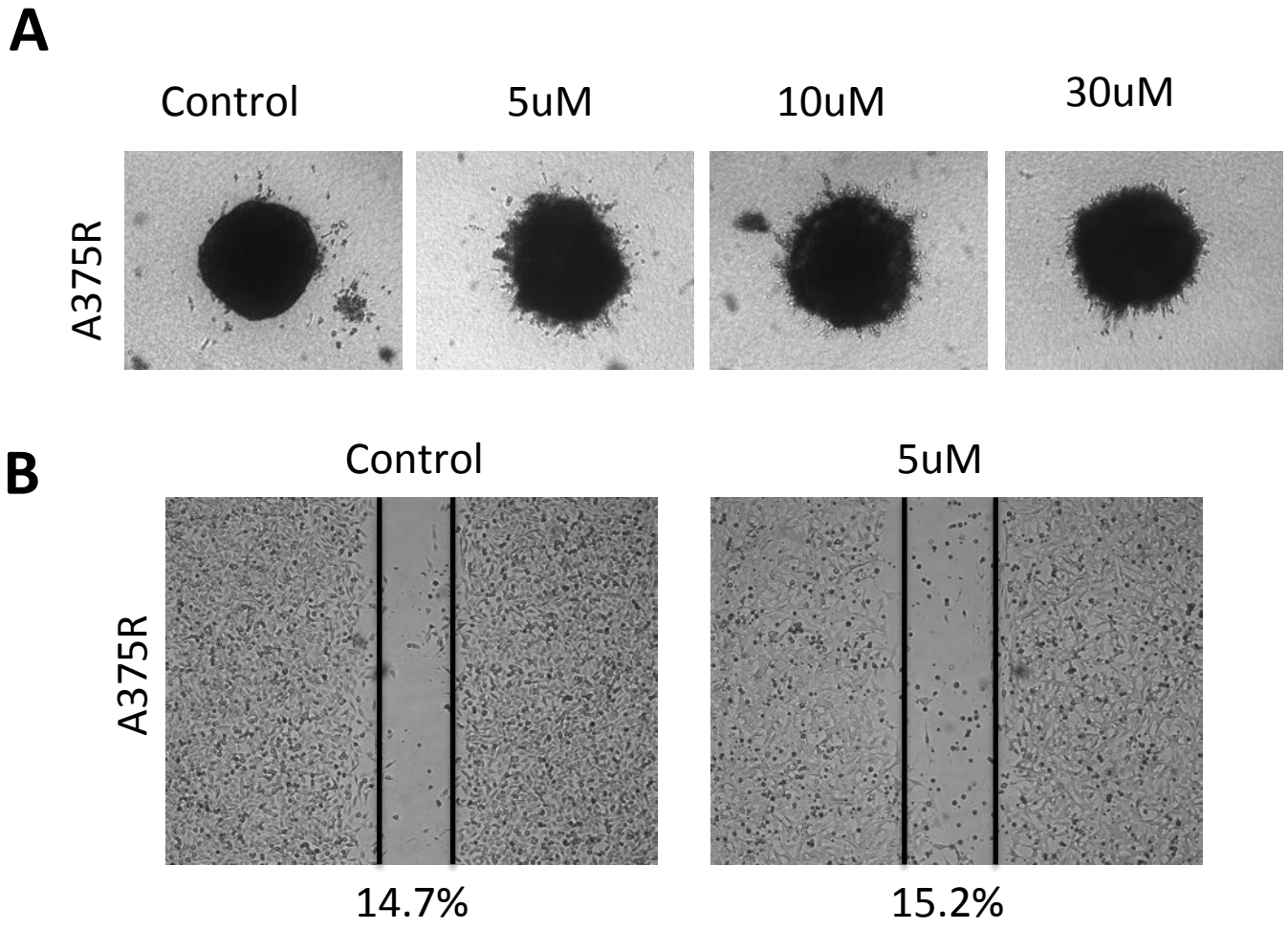

Supplementary Figure S9: FAK inhibition in FAK-inactive A375R cells. (A) 3D Spheroid invasion assay shows no inhibition of invasion in A375R cells with increasing doses of FAKi PF573228. **(B)** Wound healing assay shows nearly no inhibition of migration in A375 with FAKi after 24 hours. Values represent the percentage of scratch surface area (not covered by cells).